Random Walk evaluation of Green's functions for groundwater flow in heterogeneous aquifers

Tongchao Nan[1], Jichun Wu[1], Alberto Guadagnini[2], Xiankui Zeng[1] and Xiuyu Liang[3,4]

[1]Key Laboratory of Surficial Geochemistry of Ministry of Education, School of Earth Sciences and Engineering, Nanjing University, Nanjing 210023, China.

[2]Dipartimento di Ingegneria Civile e Ambientale (DICA), Politecnico di Milano, Piazza Leonardo da Vinci 32, 20133 Milano, Italy.

[3]Guangdong Provincial Key Laboratory of Soil and Groundwater Pollution Control, School of Environmental Science and Engineering, Southern University of Science and Technology, Shenzhen 518055, China.

[4]State Environmental Protection Key Laboratory of Integrated Surface Water-Groundwater Pollution Control, School of Environmental Science and Engineering, Southern University of Science and Technology, Shenzhen 518055, China.

Corresponding authors: Tongchao Nan (tcnan@nju.edu.cn); Jichun Wu (jcwu@nju.edu.cn)

Highlights:

- Quantitative link between WOG and Green's function for groundwater flow is found.
- Performance is assessed in five test cases with increased level of complexity.
- The method is applicable to heterogeneity, various boundary conditions and forcing.

Abstract

The use of the Walk on Grid (WOG) approach for the reliable evaluation of the Green's function associated with groundwater flow scenarios in heterogeneous geologic media is explored. The study rests on the observation that, while the Green's function method (GFM) is one of the most significant and convenient approaches to tackle groundwater flow, Green's function evaluation is fraught with remarkable difficulties in the presence of realistic groundwater settings taking place in complex heterogeneous geologic formations. Here WOG approach is used to simulate pressure dissipation by lattice random walk and establish a quantitative relationship between space-time distribution of random walkers and the Green's function associated with the underlying flow problem. WOG-based Green's function method is tested (*a*) in three scenarios where analytical formulations are available for the Green's function and (*b*) in two groundwater flow systems with increased level of complexity. Our results show that WOG can (*a*) accurately evaluate the Green's function, being highly efficient when the latter can be analytically expressed in terms of infinite series; and (*b*) accurately and efficiently evaluate temporal evolutions of hydraulic heads at target locations in the heterogeneous systems. As such, a WOG-based approach can be employed as an efficient surrogate model in scenarios involving groundwater flow in complex heterogeneous domains.

1 Introduction

The Green's function method (GFM) is a convenient and powerful approach to solve a variety of environmental and earth science problems. Its applications in the context of groundwater flow scenarios are wide and numerous, including head calculation, permeability scaling, uncertainty quantification, moment equation solving, subsurface imaging, superimposition in time domain etc. (see, *e.g.*, amongst others, Borcea et al., 2002; Dagan, 1989; Gomez & Torres-Verdin, 2019; Hristopulos & Christakos, 1999; Lembcke et al., 2016; Liu & Ball, 1998; Naff & Vecchia, 1986; Nan et al., 2019; Neuman & Orr, 1993; Olsthoorn, 2008; Park & Zhan, 2001; Sanskrityayn et al., 2017; Zhang, 2001). A key strength of the approach is that the evaluation of the Green's function for a given set of boundary types enables one to tackle a large variety of related flow scenarios subject to diverse strengths of the corresponding boundary terms and a (potentially unlimited) range of source terms, a feature which is appealing in the context of water management practices. Evaluation of the Green's function also yields insights about the relative strength of the (possibly competing) effects of diverse source terms on a target state variable throughout the system.

In many groundwater problems, one is not interested in evaluating hydraulic heads everywhere in a subsurface formation and is otherwise focused on hydraulic heads at a few specified locations, for engineering and/or environmental studies. For example, hydraulic heads from some observation wells are used as constraints or references in contaminant source identification / aquifer parameter estimation/ aquifer management (see, *e.g.*, Ayvaz & Karahan, 2008; Cheddadi, 2007; Hou & Lu, 2018; Liang & Zhang, 2012; McKinney & Lin, 1994; Saffi & Liu et al., 2015). For such cases, solutions formulated in terms of Green's function can constitute an efficient and convenient tool to evaluate hydraulic heads and their temporal series.

Green's functions of analytical or semi-analytical form are generally obtained through approaches based on (*a*) Laplace transform, (*b*) separation of variables, (*c*) eigen-function expansion, or (*d*) the method of images (Cole et al., 2011 and reference therein). By searching Green's function libraries (*e.g.*, Cole, 2019), one may find out whether a Green's function solution is available for a type of problems. However, dealing with practical complex domain features, such as, *e.g.*, irregular geometry and heterogeneity of system attributes, can still constitute a formidable challenge. To the best of our knowledge there is no Green's function available to assist solving groundwater flow taking place in generally heterogeneous aquifers, potentially characterized by boundaries of irregular shape. Scenarios linked to relative simple heterogeneity patterns (*e.g.*, stratified or block-heterogeneous media consisting of non-overlapping homogeneous regions) can be tackled upon relying on a series of basis functions to yield an approximate expression of Green's functions (Cole et al., 2011; Hahn & Özişik, 2012). A key weakness of this approach is that ad-hoc basis functions need to be constructed for each region forming the internal architecture of the zoned system. The increased number of such basis functions can be a highly limiting factor in media of complex zonal heterogeneity. In highly heterogeneous aquifers, classic numerical approaches like finite difference or finite element methods can be used to solve problem-dependent Green's function equation (Equation (5)) directly (Olsthoorn, 2008; Guadagnini & Neuman, 1999). However, the existence of Dirac function greatly undermines the accuracy, stability and convergence of numerical solutions of Green's functions (Barajas-Solano & Tartakovsky, 2013; Chen et al., 2007), often leading to failure of convergence during numerical calculation. The main objective of this study is to present a general numerical approach which can resolve these difficulties stably and efficiently and then assess its potential through a collection of test problems.

Backward random walk was applied to solve a diffusion-type partial differential equation (PDE) based on the Feynman-Kac theorem (Marie & Nguyen, 2016; Nan & Wu, 2018; Nan et al., 2019). Some studies pointed out the relation between the Green's function and the probability density of a walker that is absorbed at a domain boundary in homogenous media (Deaconu & Lejay, 2006; Hwang & Mascagni, 2003; and references therein), *i.e.*, in a Laplacian boundary-value problem $\Delta u(\mathbf{x})=2f(\mathbf{x})$ on a domain Ω, where $u(\mathbf{x})=\varphi(\mathbf{x})$ on boundary $\partial\Omega$. If the corresponding Green's function $G^{(s)}(\mathbf{x}\,|\,\mathbf{s})$ exists, the probability density $p_{\partial\Omega}(\mathbf{x}\,|\,\mathbf{s})$, at point $\mathbf{x}$ of a Brownian particle starting from point $\mathbf{s}$ and being absorbed at point $\mathbf{x}$ on boundary $\partial\Omega$ is given by

$$p_{\partial\Omega}(\mathbf{x}\,|\,\mathbf{s}) = -\frac{\partial G^{(s)}(\mathbf{x}\,|\,\mathbf{s})}{\partial \mathbf{n}} \quad \mathbf{x}\in\partial\Omega, \mathbf{s}\in\Omega \tag{1}$$

where $\mathbf{n}$ is an outward unit vector normal to the domain boundary and the probability of finding the particle inside the domain, $p_{\text{inside}}(\mathbf{x}\,|\,\mathbf{s})$, satisfies the diffusion equation and is proportional to Green's function $G^{(\mathrm{s})}(\mathbf{x}\,|\,\mathbf{s})$ of the problem, *i.e.*

$$p_{\text{inside}}(\mathbf{x}\,|\,\mathbf{s}) \propto G^{(\mathrm{s})}(\mathbf{x}\,|\,\mathbf{s}) \quad \mathbf{x},\mathbf{s} \in \Omega \tag{2}$$

The solution to this problem is (Deaconu & Lejay, 2006)

$$u(\mathbf{x}_0) = \int_{\Omega} p_{\text{inside}}(\mathbf{x}'\,|\,\mathbf{x}_0) f(\mathbf{x}')\mathrm{d}\mathbf{x}' + \int_{\partial\Omega} p_{\partial\Omega}(\mathbf{x}'\,|\,\mathbf{x}_0)\varphi(\mathbf{x}')\mathrm{d}v' \tag{3}$$

where v' is a spatial element (which coincides with a length or an area for one- and two-dimensional boundaries in Euclidean space, respectively) on boundary $\partial\Omega$.

For a homogenous domain with a simple geometry such as rectangles, spheres and/or cylinders, analytical forms of $G^{(\mathrm{s})}(\mathbf{x}\,|\,\mathbf{s})$ are readily available to derive $p_{\partial\Omega}(\mathbf{x}\,|\,\mathbf{s})$ and $p_{\text{inside}}(\mathbf{x}\,|\,\mathbf{s})$, thus forming the basis for random walk simulation algorithms. The latter include, *e.g.*, “Walk on Spheres” (WOS), “Walk on Rectangles” (WOR) and “Green’s function first-passage method” (GFFP) (see, *e.g.*, Muller, 1956; Deaconu & Lejay, 2006; Hwang et al., 2001; Hwang & Mascagni, 2003; Milstein & Tretyakov, 1999). Efforts have also been devoted to extend WOS and GFFP to stratified media (*e.g.*, Lejay & Matinez, 2006; Lejay & Marie, 2013; Lejay & Pichot, 2012; Marie & Nguyen, 2016). Still, these methods are mainly effective for media characterized by a relatively low number of zones/layers that are otherwise demarcated by regular (straight or circular) internal boundaries, thus being somewhat limited for routine applications to complex environmental scenarios (Lejay & Pichot, 2016).

Expressing hydraulic heads in natural aquifers through a Green's function approach entails Equations (1) and (2) to hold for general heterogeneity patterns. While noting that $p_{\partial\Omega}(\mathbf{x} \mid s)$ was analytically derived in a two-phase material for a very simplified internal geometry (Sahimi, 2003; Torquato et al., 1999), key questions that are not yet fully addressed and now being tackled in this study are of the kind "Do Equations (1) and (2) hold in media where heterogeneity patterns are not limited to some simplifying assumptions?" and "If so, how can one evaluate $G^{(s)}(\mathbf{x} \mid \mathbf{s})$ and even transient $G(\mathbf{x}, t \mid \mathbf{s}, \tau)$ effectively and accurately?"

In this study, the relation between Green's function and walker density is extended to general heterogeneous media by leveraging on the work of Nan and Wu (2018) and relying on a grid-based random walk, *i.e.*, the so-called Walk on Grid (WOG), to estimate $p_{\text{inside}}(\mathbf{x} \mid \mathbf{s})$. And $G^{(s)}(\mathbf{x} \mid \mathbf{s})$ in heterogeneous aquifers is computed by evaluating $p_{\text{inside}}(\mathbf{x} \mid \mathbf{s})$ via random walk simulations and provide test examples with increased degrees of complexity, which start from simplified settings associated with analytical Green's function formulations and then considering highly heterogeneous aquifers in the presence of generally transient flow.

The work is organized as follows. The methodology and test cases are introduced in Section 2. Section 3 is devoted to validation of our WOG-based Green's function method in five case tests. WOG-based Green's functions are firstly compared to their analytical counterparts in three simple scenarios and then applied to (*a*) estimate exchange rates between a one-dimensional unconfined heterogeneous porous medium and a river, and (*b*) calculate temporal variations of heads in a two-dimensional heterogeneous aquifer. Efficiency of our approach is discussed at the end of Section 3 and conclusions are drawn in Section 4.

2 Methodology

2.1 Governing equations of groundwater flow and Green's function solution

Three-dimensional transient groundwater flow in a fully saturated geologic medium can be described by the following equation:

$$\begin{cases} \nabla \cdot (K(\mathbf{x})\nabla h) + w(\mathbf{x},t) = S_{\mathrm{s}}(\mathbf{x})\dfrac{\partial}{\partial t}h(\mathbf{x},t) & \mathbf{x}\in\Omega \\ h(\mathbf{x},t) = H_0(\mathbf{x}) & t = 0 \\ h(\mathbf{x},t) = \varphi(\mathbf{x},t) & \mathbf{x}\in\Gamma_{\mathrm{D}} \\ K(\mathbf{x})\dfrac{\partial h}{\partial n} + b(\mathbf{x})h = r(\mathbf{x},t) & \mathbf{x}\in\Gamma_{\mathrm{R}} \end{cases} \tag{4}$$

where $h(\mathbf{x},t)$ [L] is hydraulic head; $\mathbf{x} = [x, y, z]^{\mathrm{T}}$ is spatial location vector within domain Ω; $K(\mathbf{x})$ [LT^{-1}] is hydraulic conductivity and $S_{\mathrm{s}}(\mathbf{x})$ [L^{-1}] is specific storage; $w(\mathbf{x},t)$ [T^{-1}] is a source/sink term; Γ_{D} and Γ_{R} are Dirichlet and Robin boundaries, respectively; n is the outward normal to Γ_{R}, whose direction depends on the shape of Γ_{R}.

By introducing a linear operator $\mathcal{L}(\cdot) = S_{\mathrm{s}}(\mathbf{x})\dfrac{\partial}{\partial t} - \nabla(K(\mathbf{x})\nabla\cdot)$, the first in Equation (4) is rewritten as $\mathcal{L}h(\mathbf{x},t) = w(\mathbf{x},t)$. The corresponding Green's function, G [L^{-2}], associated with Equation (4) satisfies the following auxiliary equation:

$$\begin{cases} \mathcal{L}G(\mathbf{x},t\,|\,\mathbf{s},\tau) = \delta(\mathbf{x}-\mathbf{s})\delta(t-\tau), \quad x,s \in \Omega, t > \tau \\ G(\mathbf{x},t\,|\,\mathbf{s},\tau) = 0, \quad t < \tau \\ G(\mathbf{x},t\,|\,\mathbf{s},\tau) = 0, \quad x \in \Gamma_{\mathrm{D}} \\ K(\mathbf{x})\dfrac{\partial G}{\partial n} + b(\mathbf{x})G(\mathbf{x},t\,|\,\mathbf{s},\tau) = 0, \quad x \in \Gamma_{\mathrm{R}} \end{cases} \tag{5}$$

The solution to Equation (4) can then be expressed as (Cole et al., 2011)

$$h(\mathbf{x},t) = H_{\mathrm{S}} + H_{\mathrm{R}} + H_{\mathrm{D}} + H_{\mathrm{I}} \tag{6a}$$

where

$$H_{\mathrm{S}} = \int_0^t \int_\Omega G(\mathbf{x},t\,|\,\mathbf{s},\tau)\cdot w(\mathbf{s},\tau)\mathrm{d}\mathbf{s}\mathrm{d}\tau \tag{6b}$$

$$H_{\mathrm{R}} = \int_0^t \int_{\Gamma_{\mathrm{R}}} G(\mathbf{x},t\,|\,\mathbf{s},\tau)\cdot r(\mathbf{s},\tau)\mathrm{d}v\mathrm{d}\tau \tag{6c}$$

$$H_{\mathrm{D}} = \int_0^t \int_{\Gamma_{\mathrm{D}}} K\varphi(\mathbf{s},\tau)\cdot \frac{\partial}{\partial n} G(\mathbf{x},t\,|\,\mathbf{s},\tau)\mathrm{d}v\mathrm{d}\tau \tag{6d}$$

$$H_{\mathrm{I}} = \int_\Omega G(\mathbf{x},t\,|\,\mathbf{s},0)H_0(\mathbf{s})S_{\mathrm{s}}\mathrm{d}\mathbf{s} \tag{6e}$$

Here, H_{S}, H_{R}, H_{D} and H_{I} [L] in Equations (6b-6e) represent the contributions to $h(\mathbf{x},t)$ due to source/sink term, Robin boundary, Dirichlet boundary and the initial condition, respectively. Note that Robin boundary includes Neumann boundary as a special case, *i.e.*, when $b(\mathbf{x}) = 0$.

In two- and one-dimensional problems, the dimensions of Green's functions are [L^{-1}] and [-] and the framework above still works.

2.2 Relation between expected passage frequency and Green's function

Following the Feynman-Kac theorem (see, *e.g.*, Nan & Wu, 2018; Lejay & Marie, 2013), hydraulic head at a point $\mathbf{x} \in \Omega$ can be expressed as

$$h(\mathbf{x},t) = F_{\mathrm{S}} + F_{\mathrm{R}} + F_{\mathrm{D}} + F_{\mathrm{I}} \tag{7a}$$

where

$$F_{\mathrm{S}} = \left\langle \int_{0\wedge t_{\mathrm{e}}}^{t} w(\mathbf{Z}(\tau),\tau) / S_{\mathrm{S}} \mathrm{d}\tau \mid \mathbf{Z}(t) = \mathbf{x} \right\rangle \tag{7b}$$

$$F_{\mathrm{R}} = \left\langle \int_{0\wedge t_{\mathrm{e}}}^{t} r(\mathbf{Z}(\tau),\tau) \mathrm{d}\tau \mid \mathbf{Z}(t) = \mathbf{x} \right\rangle \tag{7c}$$

$$F_{\mathrm{D}} = \left\langle \varphi(\mathbf{Z}_{\mathrm{e}}, t_{\mathrm{e}}) 1_{t_{\mathrm{e}}>0} \mid \mathbf{Z}(t) = \mathbf{x} \right\rangle \tag{7d}$$

$$F_{\mathrm{I}} = \left\langle H_0(\mathbf{Z}_{\mathrm{e}}) 1_{t_{\mathrm{e}}\le 0} \mid \mathbf{Z}(t) = \mathbf{x} \right\rangle \tag{7e}$$

where $\mathbf{Z}(t)$ [L] is an Itô process described as

$$\mathrm{d}\mathbf{Z}(t) = \left(\frac{\nabla K(\mathbf{x})}{S_{\mathrm{s}}(\mathbf{x})} \right) \mathrm{d}t + \sqrt{\frac{2K(\mathbf{x})}{S_{\mathrm{s}}(\mathbf{x})}} \mathrm{d}\mathbf{W}(t), \tag{8}$$

Here, $\mathbf{W}(t)$ [T$^{1/2}$] is a Wiener process; "exit time" t_{e} is the time at which $\mathbf{Z}(t)$ arrives at boundary for the first time; $0 \wedge t_{\mathrm{e}} = \max(0, t_{\mathrm{e}})$; $\langle \cdot \mid \mathbf{Z}(t) = \mathbf{x} \rangle$ represents expectation with respect to random $\mathbf{Z}(t)$ conditional to $\mathbf{Z}$ being at location $\mathbf{x}$ at time t. $1_{t_{\mathrm{e}}>0}$=1 if $t_{\mathrm{e}} > 0$ and 0 otherwise; similar for $1_{t_{\mathrm{e}}\le 0}$. The terms F_{S}, F_{R}, F_{D} and F_{I} [L] in Equation (7) represent the impact of sources/sinks, Robin boundary, Dirichlet boundary and initial conditions, respectively. Noting that Equation (7a) is virtually identical to Equation (6a), it follows that $F_{\mathrm{S}} \equiv H_{\mathrm{S}}$, $F_{\mathrm{R}} \equiv H_{\mathrm{R}}$, $F_{\mathrm{D}} \equiv H_{\mathrm{D}}$, and $F_{\mathrm{I}} \equiv H_{\mathrm{I}}$. In view of such equivalence, one may choose to evaluate the easier one in Equations (6) and (7). When the Green's function is easier to obtain, Equation (7) can be directly evaluated through Green's function formulation (6). For example, F_{S} in (7b) can be rendered using Green's function by

$$F_{\mathrm{S}} = \int_{\Omega}\int_{0}^{t} w(\mathbf{s},\tau) G(\mathbf{x},t \mid \mathbf{s},\tau) \mathrm{d}\tau \mathrm{d}v \,. \tag{9}$$

Conversely, if direct evaluation of Green's function is difficult, such as in irregular domains of general heterogeneity, evaluation of Equation (7) is recommended which requires a numerical approximation of the stochastic path integral. In this context, one may take $\mathbf{Z}(t)$ in Equation (7) as, *e.g.*, a simple lattice random walk (denoted as $\mathbf{Z}^{*}(t)$ in Figure 1), where the walker can jump solely to neighboring sites which coincide with centers of cells in Figure 1. An approximation of the path integral is then evaluated along the lattice random path (see, *e.g.*, Klebaner, 2005). Note that the lattice random walk $\mathbf{Z}^{*}(t)$ in Figure 1 is an approximation of the actual random walk $\mathbf{Z}(t)$. For ease of notation, the lattice random walk is hereafter termed as $\mathbf{Z}(t)$.

For a realization of the lattice random walk passing through location $\mathbf{x}$ at time *t*, one has $\int_{t-\Delta t}^{t} w(\mathbf{Z}(\tau),\tau) / S_{\mathrm{S}} \mathrm{d}\tau \approx w(\mathbf{x},t) \dfrac{\Delta V(\mathbf{x})}{C(\mathbf{x},t)}$, where $\Delta V(\mathbf{x})$ is the volume of the cell at $\mathbf{x}$; $C(\mathbf{x},t) = \dfrac{S_{\mathrm{s}} \Delta V}{\Delta t} + \sum_{i=1}^{n} C_{(i)}$, $C_{(i)}$ being hydraulic conductance between the current cell and a neighboring cell (defined later; see, C_{x-} in Section 2.3). Quantity $C(\mathbf{x},t)$ can be treated as a coefficient governing head variations under unit source impulse. Increasing the value of C yields enhanced dampening of head variations induced by water injection. The approximation above leads to the Lagrangian formulation

$$\int_{0\wedge t_e}^{t} w(\mathbf{Z}(\tau),\tau)/S_{\mathrm{S}}\mathrm{d}\tau \approx \sum_{j=1}^{N_s} w(\mathbf{Z}(t_j),t_j)\frac{\Delta V(\mathbf{Z}(t_j))}{C(\mathbf{Z}(t_j),t_j)} \tag{10}$$

where N_s is the number of time steps of the lattice random walk. Note that $C(\mathbf{x},t)$ is time-invariant, *i.e.*, $C(\mathbf{x},t) \equiv C(\mathbf{x})$, if the time interval Δt is uniform. Equation (10) can be recast into its corresponding Eulerian form

$$\int_{0\wedge t_e}^{t} w(\mathbf{Z}(\tau),\tau)/S_{\mathrm{S}}\mathrm{d}\tau \approx \sum_{m=1}^{N_t}\sum_{k=1}^{N_\Omega} I(k,m,\omega)w(\mathbf{x}_k,t_m)\frac{\Delta V(\mathbf{x}_k)}{C(\mathbf{x}_k)} \tag{11}$$

where N_Ω is the total number of cells in the computational grid; N_t is the total number of time steps in $[0,t]$; ω is the index identifying a random walk realization; the random passage frequency $I(k,m,\omega)$ is either zero or a positive integer and corresponds to the number of times the random walk realization of index ω passes through the cell of $\mathbf{x}_k$ during the time window $[t_{m-1},t_m]$. Hence, one has

$$\begin{aligned} F_{\mathrm{S}} &= \left\langle \int_{0\wedge t_e}^{t} w(\mathbf{Z}(\tau),\tau)/S_{\mathrm{S}}\ \mathrm{d}\tau \mid \mathbf{Z}(t)=\mathbf{x} \right\rangle \\ &\approx \frac{1}{N_{\mathrm{MC}}}\sum_{\omega=1}^{N_{\mathrm{MC}}}\sum_{m=1}^{N_t}\sum_{k=1}^{N_\Omega} I(k,m,\omega)w(\mathbf{x}_k,t_m)\frac{\Delta V(\mathbf{x}_k)}{C(\mathbf{x}_k)} \\ &= \sum_{m=1}^{N_t}\sum_{k=1}^{N_\Omega} \overline{I}(k,m)w(\mathbf{x}_k,t_m)\frac{\Delta V(\mathbf{x}_k)}{C(\mathbf{x}_k)} \end{aligned} \tag{12}$$

where the expected passage frequency

$$\overline{I}(k,m) = \frac{1}{N_{\mathrm{MC}}}\sum_{\omega=1}^{N_{\mathrm{MC}}} I(k,m,\omega) \tag{13}$$

represents the number of times on average the random walk passes the cell of $\mathbf{x}_k$ during time window $[t_{m-1},t_m]$.

On the other hand, according to Equation (6b) one has

$$H_{\mathrm{S}} \approx \sum_{m=1}^{N_t} \sum_{k=1}^{N_\Omega} w(\mathbf{x}_k, t_m) G(\mathbf{x}, t \mid \mathbf{x}_k, t_m) \Delta t \Delta V \ . \tag{14}$$

By recalling that $F_{\mathrm{S}} = H_{\mathrm{S}}$ and comparing Equations (12) and (14), one has

$$G(\mathbf{x}, t \mid \mathbf{x}_k, t_m) \approx \frac{1}{C(\mathbf{x}_k)\Delta t} \overline{I}(k, m) \tag{15}$$

According to Cole et al. (2011, Equation (3.89) with $\alpha = 1$), Green's functions for transient and steady-state scenarios are related as $G^{(\mathrm{s})}(\mathbf{x} \mid \mathbf{s}) = \lim_{t\to\infty} \int_0^t G(\mathbf{x}, t \mid \mathbf{s}, \tau) \mathrm{d}\tau$; the subscript "(s)" stands for steady-state. Thus, the Green's function associated with the steady-state flow formulation is

$$G^{(\mathrm{s})}(\mathbf{x} \mid \mathbf{x}_k) \approx \frac{1}{C(\mathbf{x}_k)} \sum_{m=1}^{\infty} \overline{I}(k, m) \ . \tag{16}$$

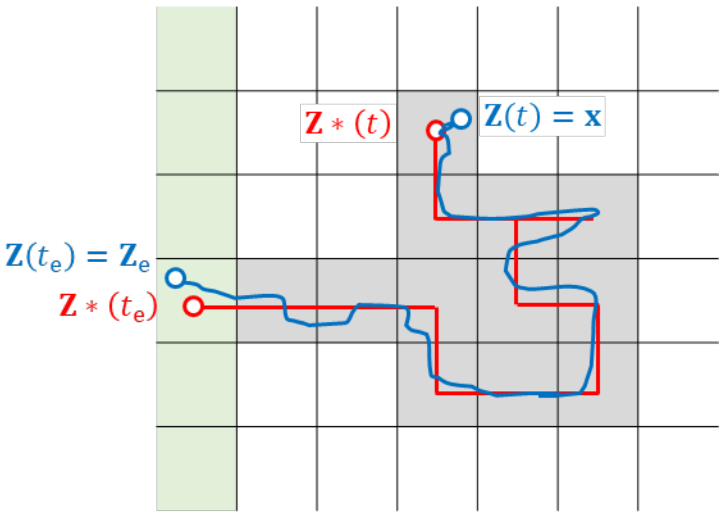

Figure 1. Lattice random walk (red) as an approximation of a general random walk (blue). Grey cells are visited by the random walks; Green cells are associated with known heads (potential exits of the walker); t_{e} is exit time, and $\mathbf{Z}_{\mathrm{e}}$ is exit location.

2.3 Numerical evaluation of Green's functions via WOG

According to Equation (7), lattice random walk realizations have to be simulated on condition that $\mathbf{Z}$ passes through location $\mathbf{x}$ at time t. Conditional simulation of $\mathbf{Z}$ realizations can be circumvented by simulating $\mathbf{Z}$ realizations backwards, as suggested by Nan and Wu (2018). In this sense, random walk realizations start at $(\mathbf{x}, t)$, trace backwards in time, and stop at $t_{\mathrm{e}} > 0$ on boundary or until $t = 0$.

Taking a three-dimensional heterogeneous aquifer as an example, simulation of a WOG realization based on Equation (4) can be performed according to the following workflow:

(1) discretize the domain into a lattice, whose nodes are centers of cells associated with a system of orthogonal coordinates (x, y, z);

(2) Let p_{x+}, p_{x-}, p_{y+}, p_{y-}, p_{z+}, and p_{z-} be the probabilities that the walker jumps from cell (i, j, k) to cells $(i+1, j, k)$, $(i-1, j, k)$, $(i, j+1, k)$, $(i, j-1, k)$, $(i, j, k+1)$, $(i, j, k-1)$, respectively, and p_{t-} be the probability that the walker stays at (i, j, k) in time window $[t_{m-1}, t_m]$. Calculate the jump probabilities as follows,

$$p_{x-} = C_{x-} / C_S, \tag{17}$$

$$p_{t-} = C_{t-} / C_S, \tag{18}$$

$$C_{t-} = \Delta V_{i,j,k} S_s / \Delta t_m , \quad (19)$$

$$C_S = C_{x-} + C_{x+} + C_{y-} + C_{y+} + C_{z-} + C_{z+} + C_{t-} ; \quad (20)$$

C_{x-} is the inter-cell conductance between cells (i, j, k) and $(i-1, j, k)$, defined as $C_{x-}=K_{(i-1);(i)} \cdot \Delta A_{(i-1);(i)} / | x_{i,j,k} - x_{i-1,j,k} |$ in McDonald and Harbaugh (1988), where $K_{(i-1);(i)}$, $\Delta A_{(i-1);(i)}$ and $| x_{i,j,k} - x_{i-1,j,k} |$ is the effective hydraulic conductivity, interface area and distance between cells (i, j, k) and $(i-1, j, k)$, respectively. Similarly, C_{x+}, C_{y-}, C_{y+}, C_{z-}, C_{z+} represent inter-cell conductance along the remaining 5 directions of a three-dimensional system. p_{x+}, p_{y-}, p_{y+}, p_{z-}, and p_{z+} can be defined similar to Equation (17). C_{t-} represents the storage-induced inertia which dampens head change in the cell; $\Delta V_{i,j,k}$ is the volume of cell (i, j, k).

(3) starting from a specific space-time point $(\mathbf{x}, t)$, randomly displace a walker to a neighboring cell according to values of local p_{x+}, p_{x-}, p_{y+}, p_{y-}, p_{z+}, p_{z-} and p_{t-}; the walker is then continuously displaced until it reaches the system boundaries or $t = 0$.

(4) simulate a large number of random walkers to estimate expected passage frequency according to Equation (13) at each cell and time step.

(5) evaluate Green's function G according to Equation (15) or (16).

Note that in steady-state problems, no initial condition exists, $p_{t-} \equiv 0$ and all random walkers will be terminated on boundary.

2.4 Five test cases

To verify WOG-based Green's functions, five test problems of groundwater flow are introduced. In the first three problems, the analytical Green's function can be found and used as references to validate WOG-based Green's functions directly. The other two problems involve pointwise heterogeneity in hydraulic parameters and no analytical Green's function are available. Thus WOG-based Green's functions are verified through their resulting hydraulic heads which are compared to numerical solutions of head calculated by the widely used MODFLOW-2000 (Harbaugh et al., 2000).

2.4.1 Test Case 1

Figure 2 presents a one-dimensional homogeneous, unconfined aquifer. Neumann and Robin boundaries are imposed at the left and right ends, respectively. Transient groundwater flow in the aquifer shown in Figure 2 is described by

$$\begin{cases} K\dfrac{\partial}{\partial x}\left(h\dfrac{\partial h}{\partial x}\right)+w_{\mathrm{u}}\left(x,t\right)=\mu\dfrac{\partial h}{\partial t} \\ \dfrac{\partial h}{\partial x}=0, \quad \text{at } x=0 \\ -Kh\dfrac{\partial h}{\partial x}=\dfrac{K_b}{2L_b}\left(h\left(L,t\right)+h_b\left(t\right)\right)\left(h\left(L,t\right)-h_b\left(t\right)\right), \quad \text{at } x=L \\ h\left(x,t\right)=H_0\left(x\right), \quad \text{at } t=0 \end{cases} \tag{21}$$

Assume that variations of h are small compared to average thickness of the aquifer. Equation (21) can be linearized and analytically solved by Green's function. More details can be found in Appendix A.

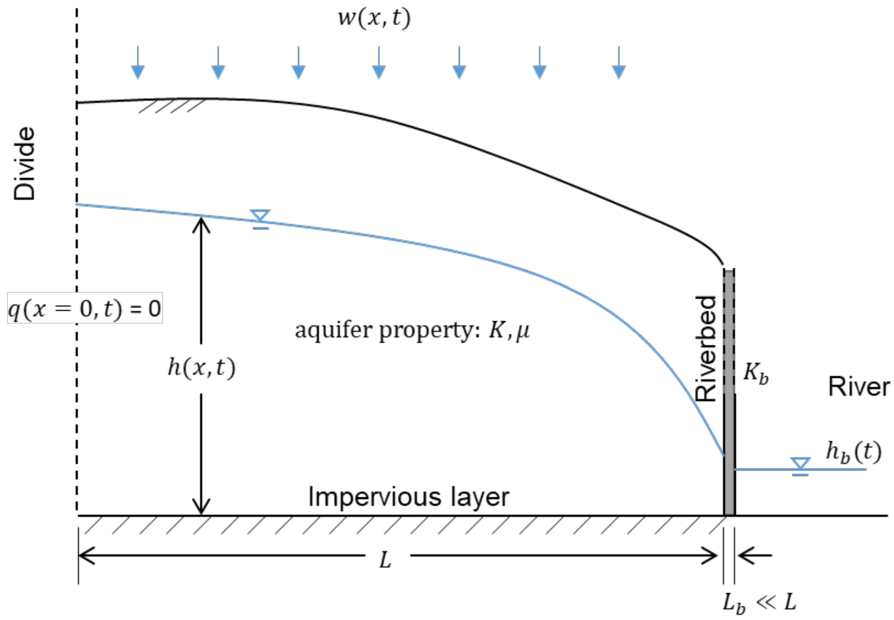

Figure 2. Conceptual model of a one-dimensional unconfined aquifer with Neumann and Robin boundaries.

2.4.2 Test Case 2

Consider two-dimensional transient flow in a homogeneous confined aquifer of size $L_x \times L_y = 1440\text{m} \times 800\text{m}$, transmissivity $T = 0.5$ m^2/d, and storativity $S = 10^{-4}$. Dirichlet boundaries are imposed at $x = 0$ and $x = 1440$ m; Neumann boundaries are set at $y = 0$ and $y = 800$ m. Analytical expressions of the Green's function are provided by Cole et al. (2011; their Equations (X11.2) and (X22.3)).

2.4.3 Test Case 3

Solving for Green's function analytically in the presence of a large number of interfaces (zones) and in higher dimensions with complex boundary conditions is problem-specified and typically challenging, especially in transient cases. For the sake of simplicity, consider a boundary-value problem in a one-dimensional aquifer, in which K may be homogeneous or block-heterogeneous. The analytical Green's function $G^{(s)}\left(x|s\right)$ corresponding to the homogeneous setting is (after Cole et al., 2011, Table X.3):

$$G^{(s)}\left(x|s\right)=\begin{cases}\left(1-\dfrac{x}{L}\right)s/K, & s<x\\ \left(1-\dfrac{s}{L}\right)x/K, & x<s\end{cases} \tag{22}$$

In the presence of multiple conductivity zones, $G^{(s)}\left(x|s\right)$ has to meet interface conditions:

$$\begin{cases}K\dfrac{\partial}{\partial s}G^{(s)}\left(x|s\right)\Big|_{s-}=K\dfrac{\partial}{\partial s}G^{(s)}\left(x|s\right)\Big|_{s+}\\ G^{(s)}\left(x|s\right)\Big|_{s-}=G^{(s)}\left(x|s\right)\Big|_{s+}\end{cases} \tag{23}$$

which are rooted in continuities of flux and hydraulic head, respectively. Expressions of $G^{(s)}\left(x|s\right)$ for two-zone and three-zone cases are shown in Section 3 below.

2.4.4 Test Case 4

Test Case 4 is a heterogeneous version of Test Case 1, in which hydraulic conductivity K and specific yield μ are point-wise heterogeneous (Figure 3 (a-b)).

Such a model is similar to the one Liang and Zhang (2013) tried to handle through analytical formulation but much more general. The natural logarithm of K is characterized by a mean value of 0.2, variance of 0.9 and an exponential variogram of integral scale of 25 m. The spatial distribution of ln$K$ is simulated by a sequential Gaussian simulator (Deutsch & Journel, 1988). K and μ are treated to be correlated according to μ=0.3+0.04$(\ln K + \xi)$, where ξ is a random variable following a standard normal distribution and correlation between ln$K$ and μ is ~0.7. Daily series of precipitation events, $R(t)$, and river stage, $h_b(t)$, are synthetically generated to reflect common hydrologic features and are depicted in Figure 3(c)-(d). The recharge coefficient varies linearly between 0.7~0.9 from x = 0 to x = L so that effective recharge to the aquifer varies spatially and temporally. To calculate the flow rate per unit width from the river to the aquifer as $q(t) = \frac{1}{2} K_b [h(L,t) + h_b(t)][h(L,t) - h_b(t)] / L_b$, head on the right end $h(x = L, t)$ is calculated by both MODFLOW-2000 and WOG. In both methods, time step length $\Delta t = 0.1\text{d}$ and discretization length $\Delta x = 0.5\text{m}$ are used.

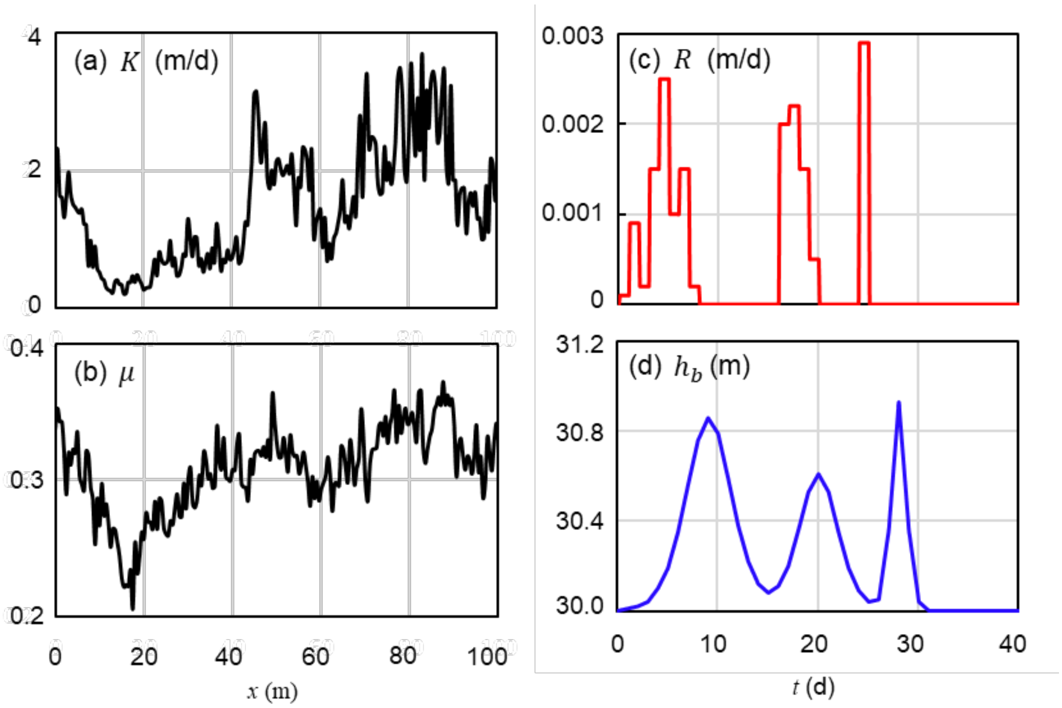

Figure 3. Spatial distribution of (a) hydraulic conductivity $K(x)$ and (b) specific yield $\mu(x)$; daily series of synthetic (c) precipitation events $R(t)$ and (d) fluctuations of river stage $h_b(t)$.

2.4.5 Test Case 5

Test Case 5 considers a horizontal two-dimensional unconfined aquifer of non-uniform hydraulic conductivity K and specific yield μ. Fields of ln$K$ with mean equal to 0.2 and variance 0.8 and μ with mean of 0.3 and variance 0.001 are independently obtained by sequential Gaussian simulation (Deutsch & Journel, 1988) using an exponential variogram of integral scale equal to 500 m. Figure 4 depicts the conceptual model of the system and maps of the spatial distribution of ln$K$ and μ. There exists an active well with pumping rate $Q(t)$ [L^3T^{-1}] and a spatially uniform but temporally varying areal recharge, $P(t)$ [LT^{-1}]. The former is located at the center of the domain, *i.e.*, at $(x_w, y_w) = (500\text{m}, 400\text{m})$, and is operated according to a prescribed time schedule (Figure 5). Two observation boreholes are set at $(x_1, y_1) = (450\text{m}, 400\text{m})$ and $(x_2, y_2) = (550\text{m}, 400\text{m})$. The East boundary is a prescribed-head boundary with head equal to $\varphi(y,t)$, the remaining boundaries being impervious. Even as both WOG and MODFLOW allow considering any functional form for $\varphi(y,t)$, we set $\varphi(y,t)$ = 50 m for simplicity. The initial head $H_0(x,y) = 50\,\text{m}$ and the study period is of 20 d.

Groundwater flow is governed by

$$\begin{cases} \dfrac{\partial}{\partial x}\left(Kh\dfrac{\partial h}{\partial x}\right) + \dfrac{\partial}{\partial y}\left(Kh\dfrac{\partial h}{\partial y}\right) + w_{\mathrm{u}}\left(x,y,t\right) = \mu\dfrac{\partial h}{\partial t} & \\ \dfrac{\partial h}{\partial x} = 0, & x = 0 \\ \dfrac{\partial h}{\partial y} = 0, & y = 0 \text{ or } L_y \\ h\left(x,y,t\right) = \varphi\left(y,t\right), & x = L_x \\ h\left(x,y,t\right) = H_0\left(x,y\right), & t = 0 \end{cases} \tag{24}$$

Here $L_x = 1000\text{m}$, $L_y = 800\text{m}$, and the total thickness is $\overline{h}$ = 50 m. $w_{\mathrm{u}}(x,y,t) = P(t) + Q(t)\delta(x_w, y_w)$. Case 5 can be numerically solved by MODFLOW-2000, or WOG-based Green's function method below.

Similar to linearization technique illustrated in Appendix A, Equation (24) can be rewritten as:

$$\begin{cases} \dfrac{\partial}{\partial x}\left(K\dfrac{\partial u}{\partial x}\right)+\dfrac{\partial}{\partial y}\left(K\dfrac{\partial u}{\partial y}\right)+2w_{\mathrm{u}}\left(x,y,t\right)=S_{\mathrm{e}}\dfrac{\partial u}{\partial t} \\ \dfrac{\partial u}{\partial x}=0,\ \text{at } x=0 \\ \dfrac{\partial u}{\partial y}=0,\ \text{at } y=0 \text{ or } L_y \\ u\left(x,y,t\right)=\varphi^2\left(y,t\right),\ \text{at } x=L_x \\ u\left(x,y,t\right)=H_0^2\left(x,y\right), \text{at } \ t=0 \end{cases} \tag{25}$$

WOG-based solution to Equation (25) is

$$u(x,y,t)=U_{\mathrm{I}}+U_{\mathrm{D}}+U_{\mathrm{S}} \tag{26a}$$

where

$$U_{\mathrm{I}}=\int_0^{L_x}\mathrm{d}x'\int_0^{L_y}H_0^2\left(x',y'\right)S_{\mathrm{e}}\left(x',y'\right)G(x,y,t\,|\,x',y',\tau=0)\mathrm{d}y', \tag{26b}$$

$$U_{\mathrm{D}}=\int_0^{t}\mathrm{d}\tau\int_0^{L_y}K\varphi^2\left(y',\tau\right)\frac{\partial}{\partial x}G(x,y,t\,|\,x'=L_x,y',\tau)\mathrm{d}y', \tag{26c}$$

$$U_{\mathrm{S}}=\int_0^{t}\mathrm{d}\tau\int_0^{L_x}\mathrm{d}x'\int_0^{L_y}2w_{\mathrm{u}}\left(x',y',\tau\right)G(x,y,t\,|\,x',y',\tau)\mathrm{d}y', \tag{26d}$$

represent the contributions to u (or equivalently, $h(x,y,t)$) of initial condition, Dirichlet boundary and source/sink terms, respectively. Recalling that $w_{\mathrm{u}}(x,y,t)=P(t)+Q(t)\delta(x_w,y_w)$, then

$U_{\mathrm{S}}=\int_0^{t}2P\left(\tau\right)\rho_P(x,y,t\,|\,\tau)\mathrm{d}\tau+\int_0^{t}2Q\left(\tau\right)\rho_Q\left(x,y,t|x_w,y_w,\tau\right)\mathrm{d}\tau$. Here,

$$\rho_P\left(x,y,t|\tau\right)=\int_0^{L_x}\mathrm{d}x'\int_0^{L_y}G(x,y,t\,|\,x',y',\tau)\mathrm{d}y' \tag{27}$$

quantifies the influence to $u\left(x,y,t\right)$ of areal recharge at time τ; and

$$\rho_Q\left(x,y,t|x_w,y_w,\tau\right)=G\left(x,y,t|x_w,y_w,\tau\right) \tag{28}$$

provides an indication of the influence to $u(x,y,t)$ of pumping at time τ at location (x_w, y_w).

If $\varphi(y,t)=\varphi(t)$ *i.e.*, independent of location, then $U_{\mathrm{D}} = \int_0^t \varphi^2(\tau)\rho_D(x,y,t\,|\,\tau)\mathrm{d}\tau$, where

$$\rho_D(x,y,t\,|\,\tau) = \int_0^{L_y} K\frac{\partial}{\partial x}G(x,y,t\,|\,x'=L_x,y',\tau)\mathrm{d}y'. \tag{29}$$

In other words, ρ_Q, ρ_P and ρ_D can be considered as the weights of source and boundary histories to impact $u(x,y,t)$. Once $G(x,y,t\,|\,x',y',\tau)$ is evaluated by WOG method, ρ_Q, ρ_P and ρ_D can be found. Afterwards, $h(x,y,t)$ can be calculated and compared to MODFLOW simulation.

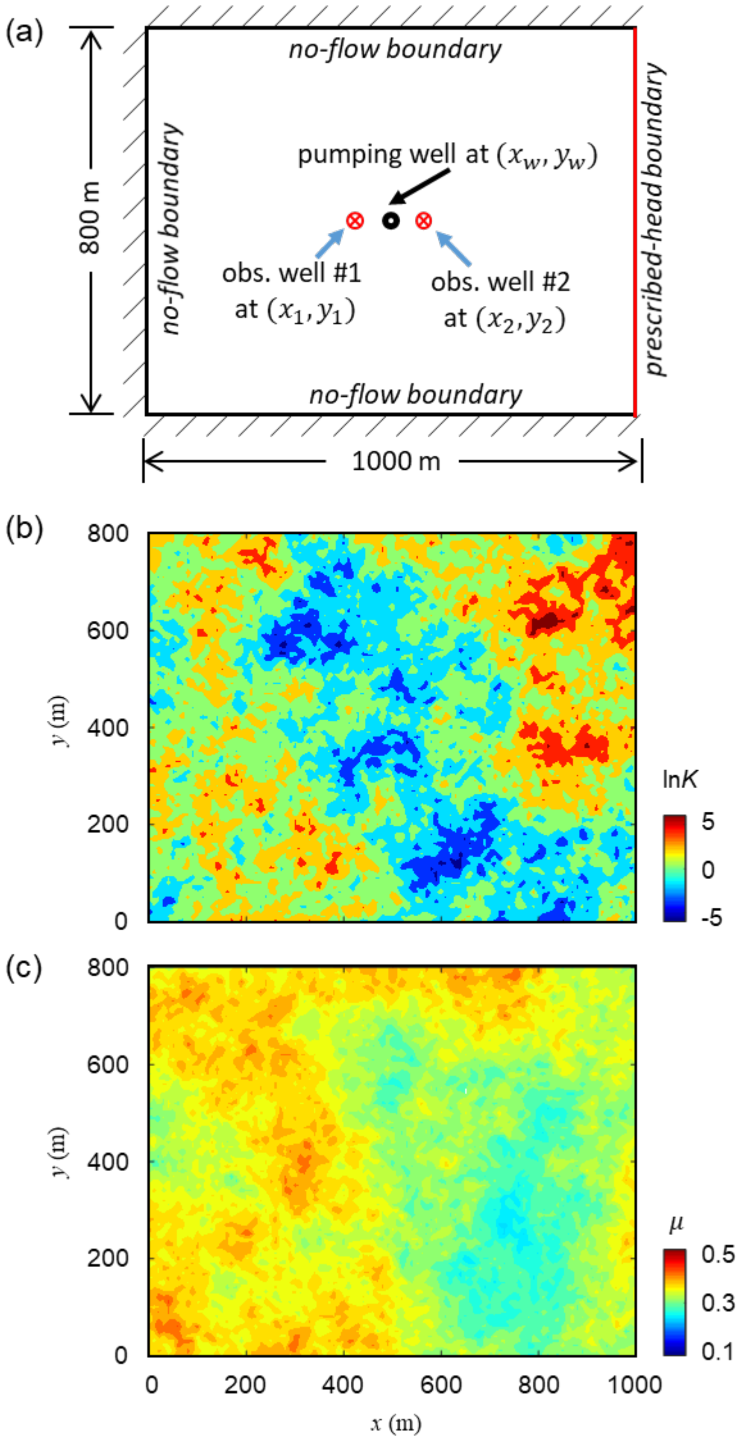

Figure 4. (a) Conceptual model of the two-dimensional unconfined aquifer; and spatial distributions of (b) hydraulic conductivity K and (c) specific yield μ.

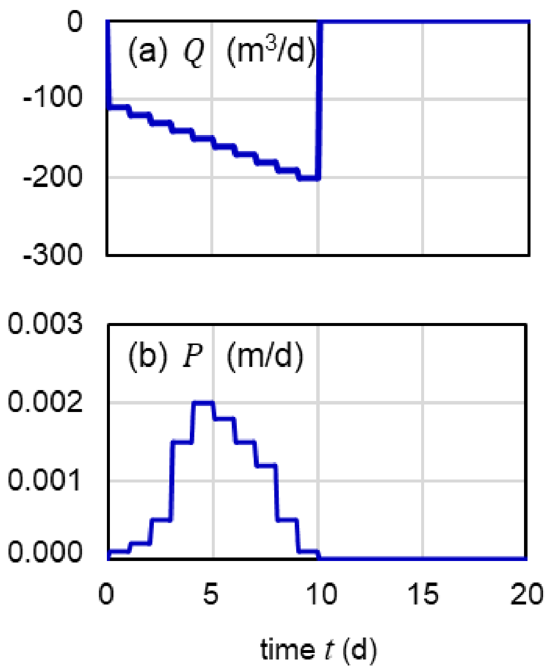

Figure 5. Time series of (a) the pumping well rate $Q(t)$ and (b) precipitation event $P(t)$.

Table 1 summarizes the dimensions of quantities mentioned in this study, which may help validate the correctness of analyses in this study.

Table 1. Dimensions of quantities in this study

variable	quantity	dimension
$\mathbf{x}$, $\mathbf{s}$	spatial vector	[L]
t, τ	time	[T]
G	transient Green's function	[L^{-2}] in 3D cases;
		[L^{-1}] in 2D cases;
		[-] in 1D cases
$G^{(s)}$	steady-state Green's function	[$L^{-2}T$] in 3D cases;

		$[L^{-1}T]$ in 2D cases;
		$[T]$ in 1D cases
L, L_x, L_y, L_z	domain size	[L]
h	hydraulic head	[L]
w	source term	$[T^{-1}]$
w_u	source term in unconfined aquifers	$[LT^{-1}]$
K	hydraulic conductivity	$[LT^{-1}]$
T	transmissivity	$[L^2T^{-1}]$
C	hydraulic conductance	$[L^2T^{-1}]$
S_S	specific storage	$[L^{-1}]$
S	storativity	[-]
μ	specific yield	[-]
S_e	depth-scaled specific yield	$[L^{-1}]$
H_S, H_R, H_D, H_I,	head due to source, Robin or Dirichlet boundary and initial condition in Green's function solution	[L]
F_S, F_R, F_D, F_I	same as above but in Feynman-Kac solution	[L]
$\mathbf{Z}(t)$	Itô process	[L]
$\mathbf{Z}^*(t)$	simple lattice random walk in space	[L]
$\mathbf{W}(t)$	Wiener process	$[T^{1/2}]$

ΔV	volume of discretization cell	[L^3]
I	passage frequency	[-]
$R(t)$, $P(t)$	precipitation rate	[LT^{-1}]
$Q(t)$	volumetric pumping rate	[L^3T^{-1}]
$q(t)$	flow rate per unit width	[L^2T^{-1}]

3 Results and Discussion

3.1 Test Case 1

WOG-based Green's function for Case 1 and its analytical counterpart are evaluated for a setting corresponding to L = 100 m, K = 1 m/d, μ = 0.3, $\overline{h} \approx$ 30 m, S_e = 0.01 m^{-1}, K_b = 0.1 m/d, L_b = 0.1 m, and a 10 days temporal window. WOG-based Green's function uses a uniform domain discretization length Δx = 0.5 m and time step length Δt = 0.05 d; the number of random walk realizations is $N_{MC} = 10^6$. On the other hand, one hundred terms are included in the evaluation of the analytical expression (Equation (A3)). Figure 6 depicts results obtained at 4 illustrative locations, x = 25 m, 50 m, 75 m, and 100 m, across the temporal range $0 < t < 10$ d. While the WOG-based results display some oscillations at low values, they virtually coincide with the analytical solution. According to Equation (15), the observed numerical errors are related to the precision of $\overline{I}$, *i.e.* $1/N_{MC}$, and are noticeable only when $\overline{I}$ is comparable to $1/N_{MC}$. On these bases, one can note that the smallest non-zero value that can be represented by Equation (15) in this example is $G = 4.9\times10^{-6}$, *i.e.*, $\ln(G) = -12.2$, which provides sufficient precision for our purpose. The location corresponding to this value corresponds to the right end in Figure 5(d), *i.e.*, the Robin boundary. This result is consistent with a dampening impact of this boundary type. Note that the Green's function at x = 100 m will always vanish when $K_b / L_b \to \infty$, in conformity with the fact that the Robin boundary tends to a Dirichlet boundary for $K_b / L_b \to \infty$. Thus, WOG-based Green's function matches its analytical counterpart with good accuracy.

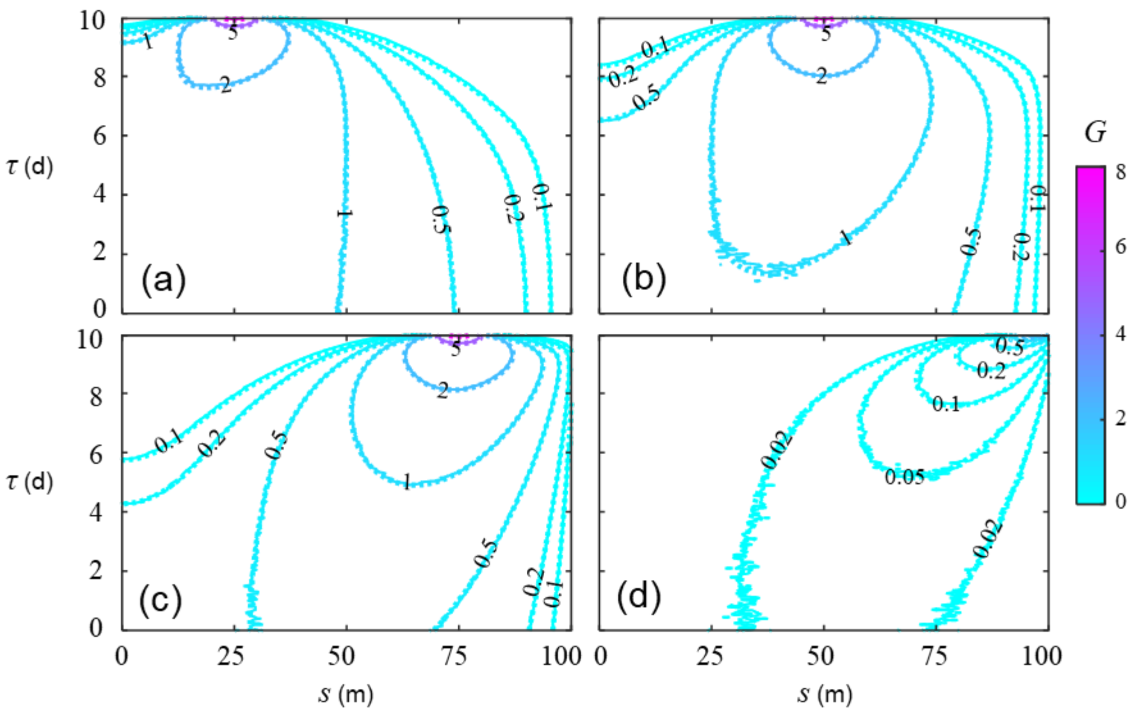

Figure 6. Transient Green's function at (a) x = 25 m; (b) x = 50 m; (c) x = 75 m, and (d) x = 100 m via analytical formulation (dashed curves) and WOG-based numerical method (solid curves).

3.2 Test Case 2

A uniform spatial discretization $\Delta x = \Delta y = 20\,\mathrm{m}$ and time step $\Delta t = 0.1$ d across a 10 days temporal window are used in WOG method. An example of the comparison between the Green's function results obtained through analytical and WOG methods is depicted in Figure 7, denoting a good agreement between them, even in the presence of some numerical errors at low values. Results of the same quality are obtained at other locations and observation times (not shown for brevity). It suggests that WOG-based Green's function is reliable.

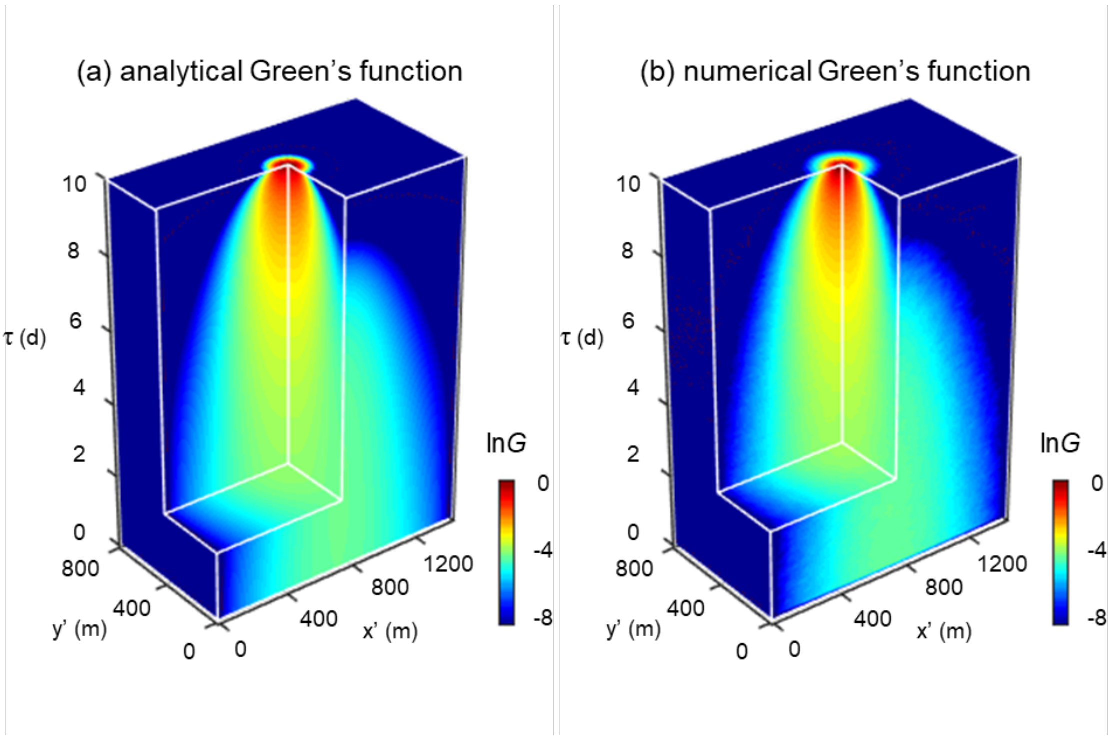

Figure 7. Logarithmic transform of $G(720\mathrm{m}, 400\mathrm{m}, 10\mathrm{d} \mid x', y', \tau)$ evaluated by (a) analytical and (b) WOG methods.

3.3 Test Case 3

By taking into account all interface conditions, mathematical expressions of Green's functions $G^{(s)}(x|s)$ in Case 3 for x = 0.15 L, 0.25 L, and 0.35 L are found and plotted in Figure 8 by red dashed lines. Corresponding WOG-based $G^{(s)}\left(x|s\right)$, obtained with a uniform domain discretization $\Delta x/L = 10^{-3}$ are also depicted by black lines. It is seen that WOG-based Green's function matches analytical counterparts very well, thus supporting the validity of Equation (16) in both homogeneous and heterogeneous media.

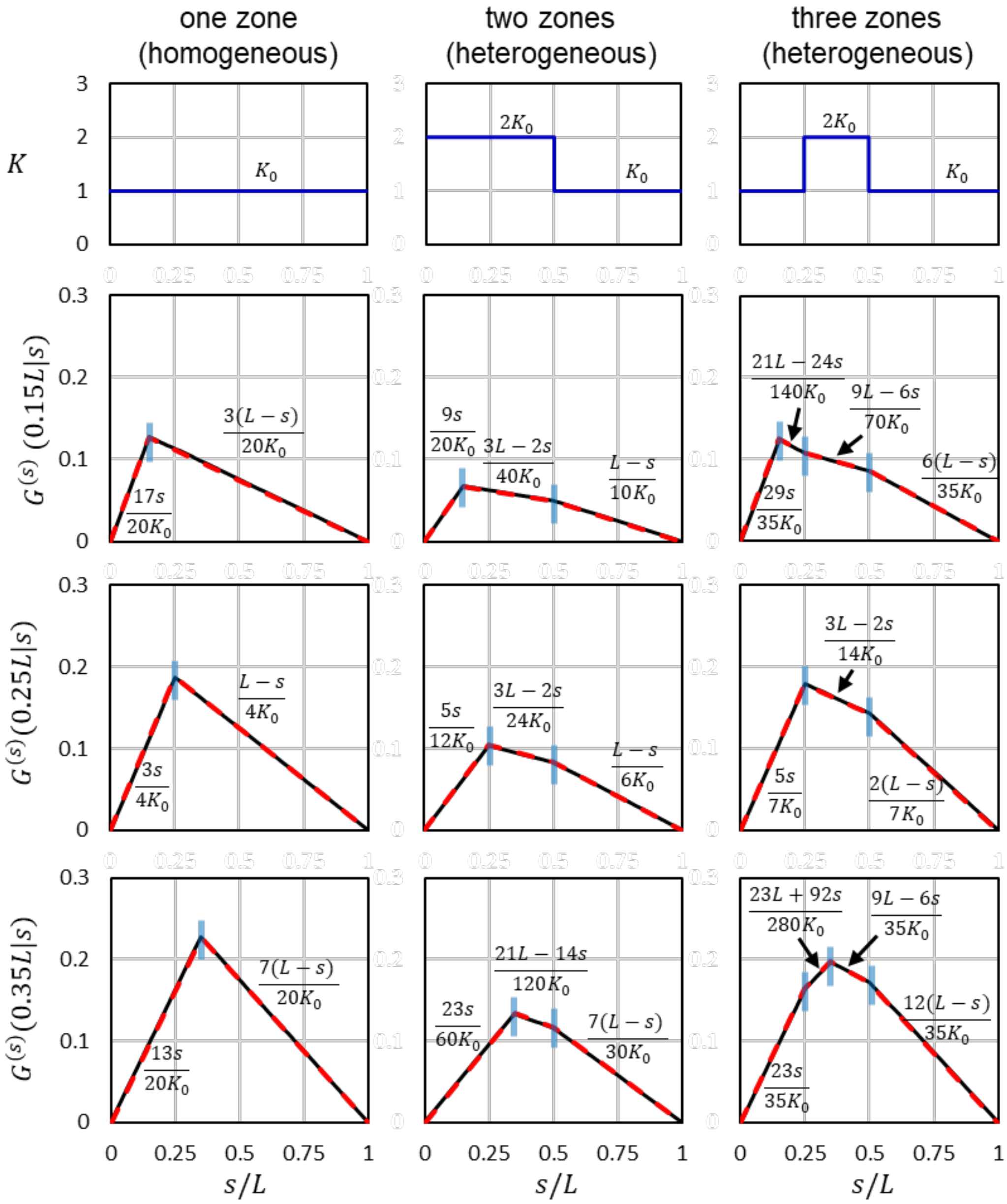

Figure 8. Analytical (red dashed) and WOG-based (black solid) Green's function for three different one-dimensional K fields, as depicted in the top row. Blue short lines show the joints of distinct segments of $G^{(s)}(x|s)$. Corresponding analytical expressions of $G^{(s)}(x|s)$ are also reported.

3.4 Test Case 4

Figure 9(a-b) reports head and flow rate at right end, $h(x = L, t)$ and $q(t)$, computed through MODFLOW and WOG-based Green's function. These results are complemented by Figure 9(c), which depicts the relative differences between $h(x = L, t)$ evaluated by WOG and MODFLOW. It is seen that differences in $h(x = L, t)$ from two methods are very limited. Results of $q(t)$ are also very close. Thus, Green's function evaluated by WOG approach is able to yield accurate solutions to groundwater flow in heterogeneous aquifers, and the effectiveness of WOG-based Green's function method is further validated.

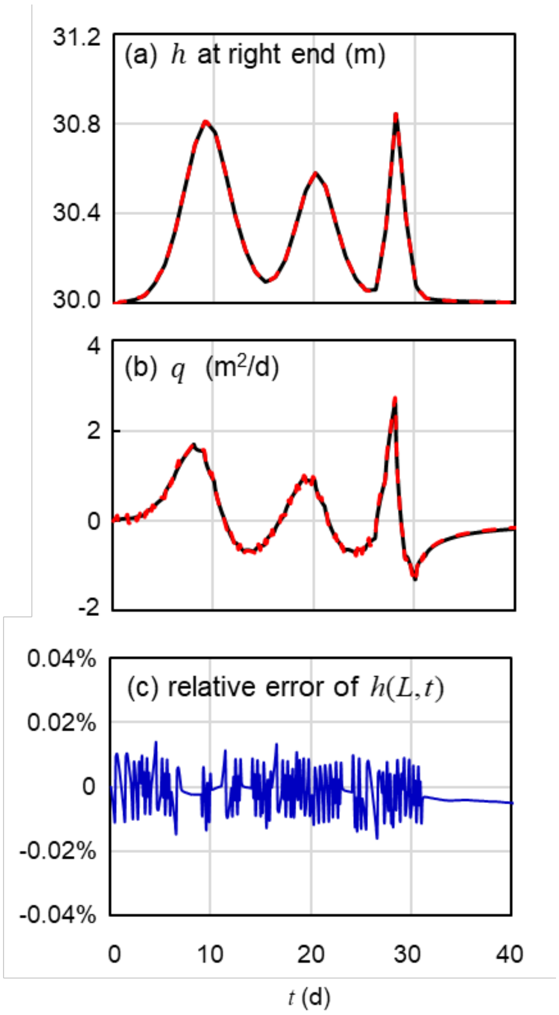

Figure 9. Results for (a) $h(L,t)$ obtained by WOG approach (black solid) and MODFLOW (red dashed); (b) aquifer-river exchange rate evaluated by WOG approach (black solid) and MODFLOW (red dashed); and (c) relative differences between $h(L,t)$ evaluated by WOG and MODFLOW.

3.5 Test Case 5

In both MODFLOW and WOG-based Green's function methods, $\Delta x = \Delta y = 10\,\text{m}$ and time step Δt = 0.1 d. Figure 10(a) depicts the WOG-based Green's function

$G(x_w, y_w, t \mid x', y', \tau)$ at the pumping well until $t = 20\,\mathrm{d}$. Figure 10(b-d) depicts spatial contours of $G(x_w, y_w, t \mid x', y', \tau)$ for $\tau \to 20\,\mathrm{d}$, $\tau = 10\,\mathrm{d}$, and $\tau = 0\,\mathrm{d}$ when $t = 20\,\mathrm{d}$.

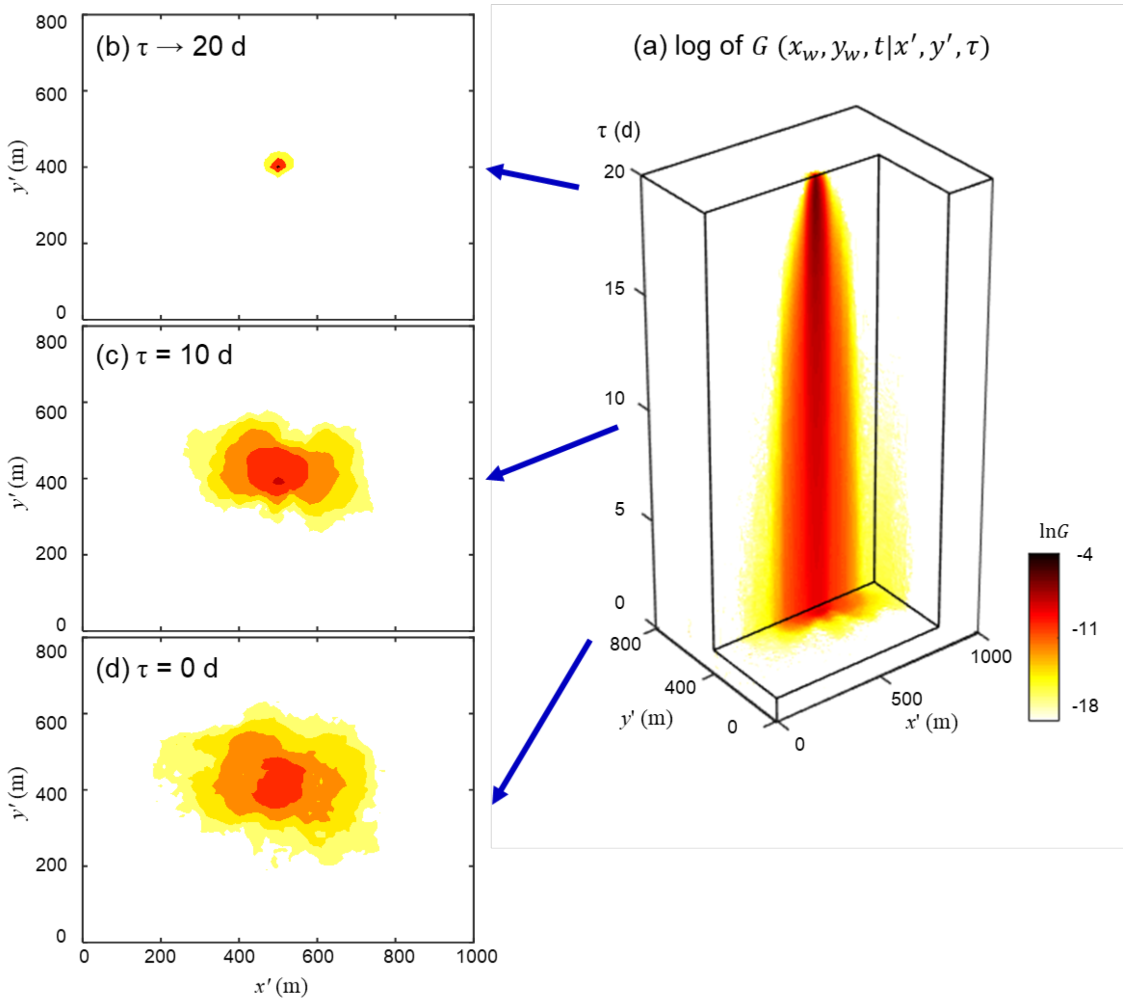

Figure 10. Natural logarithmic of the Green's function $G(x_w, y_w, t = 20\mathrm{d} \mid x', y', \tau)$ for (a) $\tau = 0 \sim 20\mathrm{d}$; the three insets correspond to contours of (b) $\tau \to 20$ d; (c) $\tau = 10$ d; and (d) $\tau = 0$ d.

Figure 11 depicts the evolution of $\rho_Q(x, y, t|x_w, y_w, \tau)$, $\rho_P(x, y, t \mid \tau)$ and $\rho_D(x, y, t \mid \tau)$ across $0 \le \tau \le t$ for $t = 20\,\mathrm{d}$ at the pumping and observation wells (Figure 4). Values of ρ_Q at the pumping well are consistently largest. It is in agreement on the fact that pumping at (x_w, y_w) naturally affects heads at (x_w, y_w) stronger than at other locations. It is also found that ρ_Q at observation well #2 is close to but greater than its counterpart evaluated at observation well #1, implying an stronger hydraulic connection between the pumping well and well #2 due to heterogeneity. According to ρ_D, the impact of Dirichlet boundary is remarkable at observation well #2 but almost negligible at observation well #1. Since ρ_Q, ρ_P and ρ_D embed point-to-point hydraulic connections in a quantitative manner, a further evolution of the study could be the analysis of the possibility to enhance our understanding about aquifer connectivity upon relying on metrics derived from a Green's function approach.

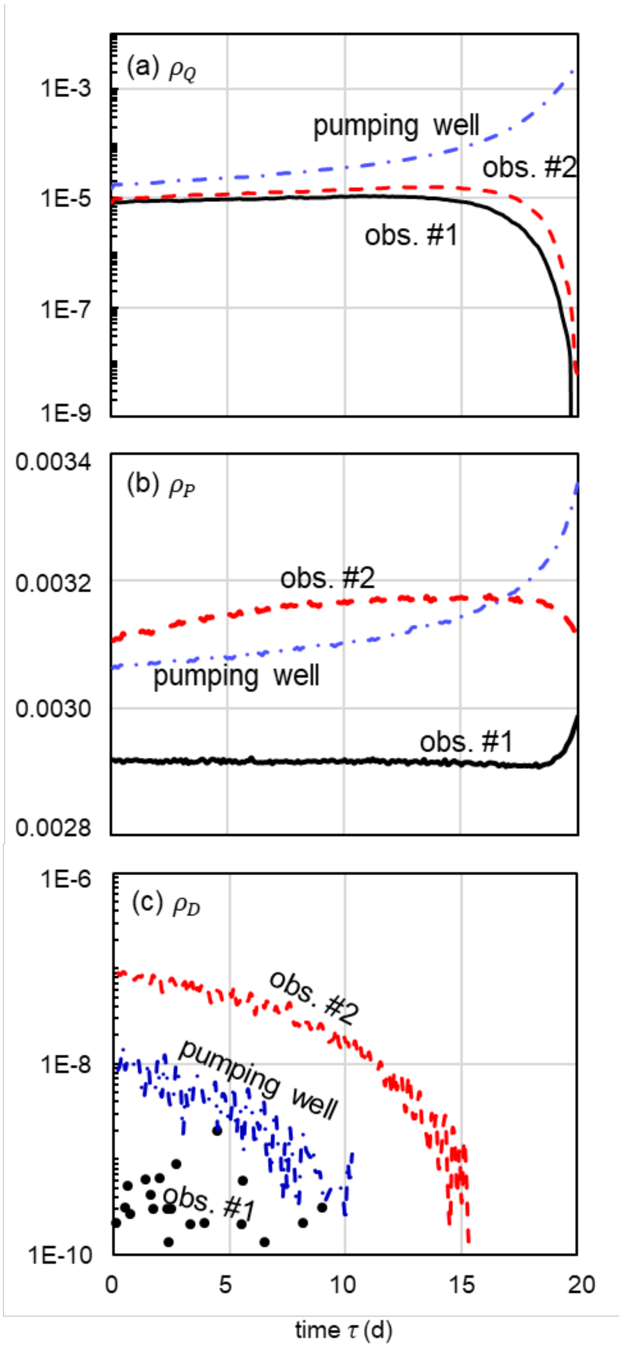

Figure 11. (a) $\rho_Q\left(x,y,t|x_w,y_w,\tau\right)$, (b) $\rho_P(x,y,t\,|\,\tau)$ and (c) $\rho_D(x,y,t\,|\,\tau)$ (see Equations (27)-(29)) for $t = 20\,\mathrm{d}$ at pumping location (x_w, y_w), and observation locations (x_1, y_1) and (x_2, y_2).

Head variation $\Delta h(x,y,t) = h(x,y,t) - H_0(x,y)$ evaluated at the two observation wells and at the pumping well are denoted as Δh_1, Δh_2 and Δh_w, respectively. Δh_1, Δh_2 and Δh_w calculated through MODFLOW and WOG are compared in Figure 12(a-c). Figure 12(d) depicts the relative differences between heads obtained by the two methods at the three target locations. These results clearly demonstrate the accuracy of the WOG-based Green's function method. Its computational costs are discussed in Section 3.6, where it is shown that WOG-based Green's function is very efficient when there is the need to assess the action of various combinations of $\varphi(y,t)$, $H_0(x,y)$, $Q(t)$ and $P(t)$, once the Green's function is found by WOG.

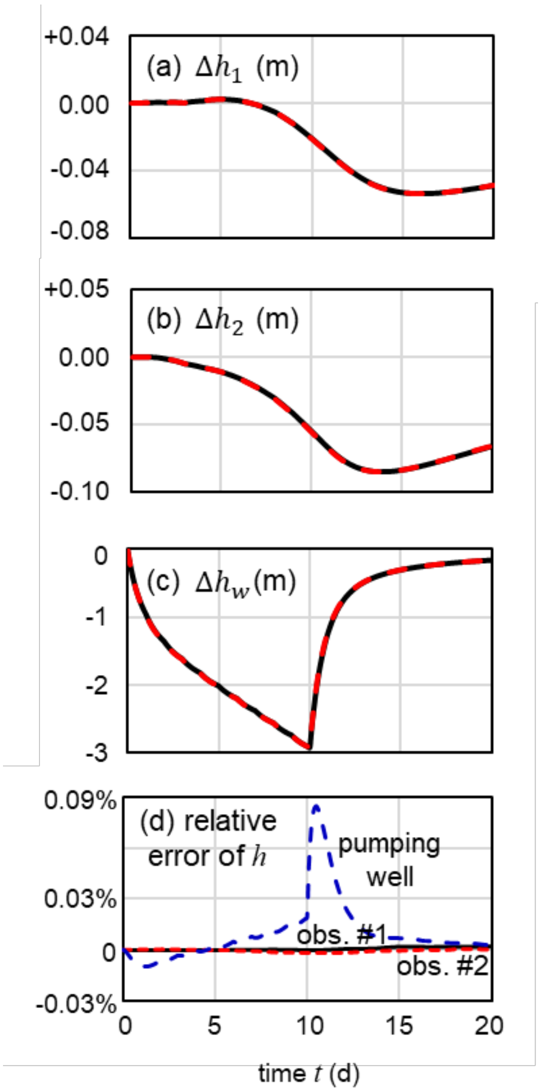

Figure 12. (a) Head variation at observation well #1, (b) at observation well #2, and (c) at pumping well (red dash: MODFLOW, black solid: WOG). (d) relative differences between heads from two methods at the three locations (blue dash: pumping well, black solid: well #1, red dash: well #2).

3.6 Advantages of WOG-based Green's function method

Two of several major advantages WOG-based Green's function approach bears are computational stability and efficiency. As mentioned in the introduction, irregularity produced by Dirac function in Green's function PDE Equation (5) often leads to difficulty in convergence and errors, which is further exacerbated by discontinuous coefficients *e.g.* hydraulic conductivities in the PDE (Barajas-Solano & Tartakovsky, 2013). Repeating failures of convergences have been observed while attempting to solve Equation (5) directly by MODFLOW. That's the reason why we don't compare Green's function from WOG to that from MODFLOW in Test Case 4 and Case 5. In contrast, WOG-based method seems work stably in all cases in our investigation here.

The second advantage is computational efficiency of this approach. It is mainly attributed to (a) parallelizability in simulating random walks and (b) framework of Green's function method which allows efficient recalculations for various combinations of boundary conditions and forcing terms.

Table 2 lists details of time costs in all of the computational studies illustrated above. For the sake of accuracy, one hundred terms are included in the evaluation of analytical expression of the Green's function in Test Case 1, a choice that yields computationally intensive evaluations. One can note that in this case the WOG-based Green's function evaluation is more efficient than its analytical counterpart. Otherwise, analytical expressions associated with Test Case 2 and Case 3 are in closed form and very efficient. In Test Case 4 and Case 5, the WOG-based approach first evaluates numerically Green's functions and then calculate hydraulic heads based on these Green's functions. The most computational cost is spent in the first step (*i.e.* Green's function evaluation) and the second step is very fast (about 10^{-2} s or less). Furthermore, the computational cost in the first step can be remarkably reduced through parallelization and more efficient than using MODFLOW.

On the other hand, MODFLOW directly solves for heads at each time step. While this computational suite is typically considered as an efficient tool, when compared to other groundwater solvers, one can see that it is still not fast enough in many scenario simulations which may require calling solver routines a large number of times. For example, addressing data assimilation, uncertainty analysis, and/or source identification problems (see, *e.g.*, Ayvaz & Karhan, 2008; Nan & Wu, 2011; Wu & Zeng, 2013; Yeh, 2015) in the presence of uncertain forcing terms and/or boundary conditions often requires relying on a high number of direct solutions of the flow scenarios. As such, surrogate models are developed to speed up the solution, often at the cost of a decreased accuracy (see, *e.g.*, Asher et al., 2015 and references therein).

When considering a WOG-based Green's function approach, performing multiple calls to scenario simulation (the second step above) is only a marginal issue because the first step (*i.e.*, Green's function evaluation) needs to be implemented only once and the computational cost of the second step is negligible. Therefore, our results evidence the potential benefit (in terms of computational cost) of relying on a WOG-based Green's function approach when there is the need for a high number of repeated solutions of the groundwater flow problem, as driven by uncertain forcing and/or boundary terms.

Table 2. Summary of the analyses performed in this study and their computational time costs

test case	dimension	transient	heterogeneous?	reference time cost (in seconds)		WOG time cost (in seconds)	
				method used	time cost	serial	parallel
1	1D	Yes	No	AGF*	~ 1200	~243	18
2	2D	Yes	No	AGF*	~ 1	~ 87	11
3	1D	No	Yes (zoned)	AGF*	negligible	~ 10	8
4	1D	Yes	Yes	MODFLOW	~ 4	~100	8
5	2D	Yes	Yes	MODFLOW	~ 25	~215	17

* AGF stands for analytical Green's function.

4 Conclusions

This study leads to the following major conclusions.

1. The relation between Green's functions and random walk is extended to heterogeneous aquifers upon deriving a quantitative relationship between Green's function and expected passage frequency of random walk. This enables one to numerically evaluate Green's functions of groundwater flow problems in aquifer systems of complex geometries and spatial heterogeneity patterns. This new method rests on the Walk on Grid (WOG) approach and its capabilities are illustrated through a suite of five test scenarios involving steady-state and transient flow, various boundary conditions, the action of spatially and/or temporally varying source terms of various nature, as well as diverse spatial distributions of system attributes *e.g.*, hydraulic conductivity and storativity.
2. Numerical Green's functions calculated by WOG are compared against exact analytical solutions under a variety of settings. Results (Figures 6, 7 and 8) show that the WOG-based Green's functions are virtually indistinguishable from their analytical counterparts, an exception being given by values that are too low to be properly captured by expected passage frequency of random walk. Numerical errors in the WOG-based evaluation of Green's functions are controlled by the precision associated with the calculated expected passage frequency $\overline{I}$, which, in turn, depends on the number of random walk realizations *i.e.*, N_{MC}. One million

realizations are used in all of our examples, which is shown to be sufficient to capture the main information in Green's functions.

3. The findings corresponding to settings of increased level of complexity where analytical solutions are not available reveal that relative differences between heads calculated via our WOG-based approach and their counterparts based on numerical solution of the widely tested computational suite MODFLOW are very small (*i.e.*, <0.02% in Figure 9(c) and <0.09% in Figure 12(d)). These results strengthen our confidence on the accuracy of WOG-based Green's functions for groundwater flow scenarios.

4. As compared against available analytical formulations, the WOG approach may be computationally more efficient in the evaluation of Green's functions when the former are expressed in terms of infinite series.

5. The WOG-based Green's function method avoids limitations of applicability to complex media which are typical of traditional approaches to the numerical evaluation of Green's functions, *i.e.*, it can efficiently handle various combinations of boundary conditions and forcing and is applicable to aquifers of general heterogeneous structure with excellent accuracy.

6. While WOG-based Green's function method appears to be more computationally demanding than MODFLOW, it is recalled that evaluation of heads is associated with negligible computational time once the Green's function is calculated. Thus, in terms of computational cost, the potential benefit of relying on a WOG-based Green's function method tends to increase when one has to perform a high number of repeated solutions of the groundwater flow problem, as driven by uncertain forcing and/or boundary terms. Potential application examples in this context, which one could consider on future studies, include the assessment of the evolution of groundwater resources as driven by various climatic scenarios, or the quantification of the sustainability of multiple extraction scenarios in a given aquifer system.
7. Finally, this study allows discriminating clearly the contributions to head distributions due to boundary and source terms. On these bases, our results form the basis upon which one can build future studies to analyze the concept of aquifer connectivity through metrics derived from a Green's function method.

Acknowledgments, Samples, and Data

This work is funded by the National Natural Science Foundation of China (Grant Nos. 41972245, 41602250), China Postdoctoral Science Foundation (Grant No. 2017M611782) and the Fundamental Research Funds for the Central Universities (Grant Nos. 0206-14380032 and 0206-14380091). Part of the work was developed while Prof. A. Guadagnini was at the University of Strasbourg with funding from Région Grand-Est and Strasbourg-Eurométropole through the 'Chair Gutenberg'. We declare that we have no conflict of interest. Data included in this study can be downloaded at: https://www.researchgate.net/profile/Tongchao_Nan/publications.

Appendix A.

We assume that the total saturated thickness is much larger than the amplitude of spatiotemporal variations of head. Setting $h^2 = u$ and $S_e = \mu / \bar{h}$ (where $\bar{h}$ is the spatially averaged saturated thickness, whose temporal variation we take as much smaller than $\bar{h}$), Equation (23) can be linearized as

$$\begin{cases} \dfrac{\partial^2 u}{\partial x^2} + \dfrac{2w(x,t)}{K} = \dfrac{S_e}{K}\dfrac{\partial u}{\partial t} \\ \dfrac{\partial u}{\partial x} = 0, \quad x = 0 \\ K\dfrac{\partial u}{\partial x} + \dfrac{K_b}{L_b}u(x,t) = \dfrac{K_b}{L_b}h_b^2(t), \quad x = L \\ u(x,t) = H_0^2(x), \quad t = 0 \end{cases} \tag{A1}$$

Boundary conditions can be recast as: $\alpha_i \frac{\partial u}{\partial x}|_{x=x_i} + \beta_i u\left(x_i, t\right) = \gamma_i\left(t\right)$, with $x_1 = 0$, $\alpha_1 = 1$, $\beta_1 = 0$, $\gamma_1 = 0$; $x_2 = L$, $\alpha_2 = K$, $\beta_2 = \frac{K_b}{L_b}$, $\gamma_2 = \frac{K_b}{L_b} h_b^2\left(t\right)$.

The solution of Equation (A1) can be expressed as

$$\begin{aligned} u\left(x,t\right) &= \int_0^L H_0^2\left(s\right) G(x,t \mid s, \tau = 0) S_{\mathrm{e}} \mathrm{d}s \\ &+ 2\int_0^t \mathrm{d}\tau \int_0^L w\left(s,\tau\right) G(x,t \mid s,\tau) \mathrm{d}s \\ &+ \int_0^t \mathrm{d}\tau \left(\sum_{i=1}^{2} \frac{\gamma_i\left(\tau\right)}{\alpha_i} G(x,t \mid s = x_i, \tau) \right) \end{aligned} \tag{A2}$$

where

$$G\left(x,t|s,\tau\right) = \frac{2}{S_{\mathrm{e}} L} \sum_{m=1}^{\infty} \exp\left(-\frac{\lambda_m^2 K\left(t-\tau\right)}{S_{\mathrm{e}} L^2} \right) \frac{\lambda_m^2 + D^2}{\lambda_m^2 + D^2 + D} \cos\left(\lambda_m \frac{x}{L}\right) \cos\left(\lambda_m \frac{s}{L}\right) \tag{A3}$$

λ_m being the m-th root of $\lambda_m \tan\left(\lambda_m\right) = D$ with $D \equiv \frac{2\beta_2 L}{K} = \frac{2K_b L}{L_b K}$.

References

Ayvaz, M.T. and Karahan, H. 2008. A simulation/optimization model for the identification of unknown groundwater well locations and pumping rates. Journal of Hydrology, 357(1-2): 76-92. DOI: 10.1016/j.jhydrol.2008.05.003.

Asher, M. J., B. F. W. Croke, A. J. Jakeman, and L. J. M. Peeters (2015), A review of surrogate models and their application to groundwater modeling, Water Resources Research, 51, 5957–5973. DOI: 10.1002/2015WR016967.

Barajas-Solano, D.A., Tartakovsky, D.M. 2013. Computing Green's Functions for Flow in Heterogeneous Composite Media. International Journal for Uncertainty Quantification, 3(1):39-46. DOI: 10.1615/Int.J.UncertaintyQuantification.2012003671.

Borcea, L., Papanicolaou, G., Tsogka, C., Berryman, J. 2002. Imaging and time reversal in random media. Inverse Problems, 18(5):1247. DOI: 10.1088/0266-5611/18/5/303.

Chen, L., Holst, M.J., Xu, J. 2007. The finite element approximation of the nonlinear Poisson-Boltzmann equation. SIAM Journal of Numerical Analysis. 45(6): 2298-2320. DOI: 10.1137/060675514.

Cole, K.D. 2019. Green's Function Library. http://www.greensfunction.unl.edu/home/index.html. Last access on 2019/5/5.

Cole, K.D., Beck, J.V., Haji-Sheikh, A., Litkouhi, B. 2011. Heat conduction using Green's functions. 2nd edition. CRC Press. ISBN: 143981354X.

Deaconu, M., Lejay, A., 2006. A Random Walk on Rectangles Algorithm. Methodology and Computing in Applied Probability. 8: 135-151. DOI: 10.1007/s11009-006-7292-3.

Dagan, G. 1989. Flow and Transport in Porous Formations. Springer-Verlag, Berlin Heidelberg.

Deutsch, C.V. and Journel, A.G. 1998. GSLIB Geostatistical Software Library and User's Guide, 2nd ed. Oxford University Press, Oxford. DOI: 10.2307/1270548.

Gomez, J.D.E, Torres-Verdin, C. 2019. Permeability sensitivity functions and rapid simulation of multi-point pressure measurements using perturbation theory. Advances in Water Resources, 129: 198-209. DOI: 10.1016/j.advwatres.2019.05.015.

Guadagnini, A., Neuman, S.P. 1999. Nonlocal and localized analyses of conditional mean steady state flow in bounded, randomly nonuniform domains. 1. Theory and computational approach. Water Resources Research, 35(10): 2999-3018. DOI: 10.1029/1999WR900160.

Hahn, D.W. and Özişik, M.N. 2012. Heat Conduction, Third Edition. John Wiley & Sons, INC. Hoboken, New Jersey. DOI:10.1002/9781118411285.

Harbaugh, A.W., Banta, E.R., Hill, M.C., Mcdonald, M.G. 2000. MODFLOW-2000, the U.S. geological survey modular ground-water flow model-User guide to modularization concepts and the ground-water flow process. U.S. Geol. Surv. Open File Rep., 00-92.

Hristopulos, D. T., Christakos, G. 1999. Renormalization group analysis of permeability upscaling. Stochastic Environmental Research and Risk Assessment, 13(1-2): 131-160. DOI: 10.1007/s004770050036.

Hou, Z.Y. and Lu, W.X. 2018. Comparative study of surrogate models for groundwater contamination source identification at DNAPL-contaminated sites. Hydrogeology Journal. 26(3):923-932. DOI: 10.1007/s10040-017-1690-1.

Hwang, C. O., Given, J. A., Mascagni, M. 2001. The simulation-tabulation method for classical diffusion Monte Carlo. Journal of Computational Physics. 174(2): 925-946. DOI: 10.1006/jcph.2001.6947.

Hwang, C.O. and Mascagni, M., 2003. Analysis and comparison of Green's function first-passage algorithms with "Walk on Spheres" algorithms. Mathematics and Computers in Simulation. 63(6): 605-613. DOI: 10.1016/S0378-4754(03)00091-0.

Klebaner, F.C. 2005. Introduction to Stochastic Calculus with Applications, Second Edition. Imperial College Press. London, UK. ISBN: 9781848168312.

Lejay A., Marie S., 2013. New Monte Carlo schemes for simulating diffusions in discontinuous media. Journal of Computational and Applied Mathematics. 245: 97-116. DOI: 10.1016/j.cam.2012.12.013.

Lejay A., Martinez, M., 2006. A scheme for simulating one-dimensional diffusion processes with discontinuous coefficients. Annals of Applied Probability. 16(1): 107-139. DOI: 10.1214/105051605000000656.

Lejay, A., Pichot, G., 2012. Simulating diffusion processes in discontinuous media: a numerical scheme with constant time steps. Journal of Computational Physics. 231(21): 7299-7314. DOI: 10.1016/j.jcp.2012.07.011.

Lejay, A., Pichot, G., 2016. Simulating diffusion processes in discontinuous media: Benchmark tests. Journal of Computational Physics. 314: 384-413. DOI: 10.1016/j.jcp.2016.03.003.

Lembcke, L.G.M., Roubinet, D., Gidel, F., Irving, J., Pehme, P., Parker, B.L. 2016. Analytical analysis of borehole experiments for the estimation of subsurface thermal properties. Advances in Water Resources, 91:88-103. DOI: 10.1016/j.advwatres.2016.02.011.

Liu C.X. and Ball W.P. 1998. Analytical modeling of diffusion-limited contamination and decontamination in a two-layer porous medium. Advances in Water Resources. 21(4): 297-313. DOI: 10.1016/S0309-1708(96)00062-0.

Liu, H. J., Hsu, N. S., Yeh, W. W. G. 2015. Independent component analysis for characterization and quantification of regional groundwater pumping. Journal of Hydrology. 527: 505-516. DOI: 10.1016/j.jhydrol.2015.05.013.

Liang, X.Y. and Zhang, Y.K. 2012. A new analytical method for groundwater recharge and discharge estimation. Journal of Hydrology. 450-451: 17-24. DOI: 10.1016/j.jhydrol.2012.05.036.

Liang, X.Y. and Zhang, Y.K. 2013. Analytic solutions to transient groundwater flow under time-dependent sources in a heterogeneous aquifer bounded by fluctuating river stage. Advances in Water Resources. 58: 1-9. DOI: 10.1016/j.advwatres.2013.03.010.

McDonald, M.G., Harbaugh, A.W., 1988. A modular three-dimensional finite-difference ground-water flow model: U.S. Geological Survey Techniques of Water-Resources Investigations, book 6, chap. A1. 586p.

McKinney, D.C. and Lin, M.D. 1994. Genetic Algorithm Solution of Groundwater-Management Models. Water Resources Research. 30(6): 1897-1906. DOI: 10.1029/94WR00554.

Muller, M.E., 1956. Some continuous Monte Carlo methods for the Dirichlet problem. Annals of Mathematical Statistics. 27: 569-589. DOI: 10.1214/aoms/1177728169.

Milstein, G.N., Tretyakov, M.V., 1999. Simulation of a space-time bounded diffusion. Annals of Applied Probability, 9(3): 732-779.

Maire, S., Nguyen, G., 2016. Stochastic finite differences for elliptic diffusion equations in stratified domains. Mathematics and Computers in Simulation, 121: 146-165. DOI: 10.1016/j.matcom.2015.09.008.

Naff, R. L. and Vecchia, A. V. 1986. Stochastic-Analysis of 3-Dimensional Flow in a Bounded Domain. Water Resources Research. 22(5): 695-704. DOI: 10.1029/WR022i005p00695.

Nan, T.C., Wu, J.C., Li, K.X., Jiang, J.G. 2019. Permeability estimation based on the geometry of pore space via random walk on grids. Geofluids. 2019. DOI: 10.1155/2019/9240203.

Nan, T.C. and Wu, J.C. 2018. Random walk path solution to groundwater flow dynamics in highly heterogeneous aquifers. Journal of Hydrology. 563: 543-559. DOI: 10.1016/j.jhydrol.2018.05.008.

Nan, T.C. and Wu, J.C. 2011. Groundwater parameter estimation using the ensemble Kalman filter with localization. Hydrogeology Journal. 19(3): 547-561. DOI: 10.1007/s10040-010-0679-9.

Neuman, S.P., Orr, S. 1993. Prediction of Steady-State flow in Nonuniform Geologic Media by Conditional Moments: Exact Nonlocal Formalism, Effective Conductivities, and Weak Approximation. Water Resources Research, 29(2):341-364. DOI: 10.1029/92WR02062.

Olsthoorn, T.N. 2008. Do a bit more with convolution. Groundwater, 46(1): 13-22. DOI: 10.1111/j.1745-6584.2007.00342.x.

Park, E. and Zhan, H.B. 2001. Analytical solutions of contaminant transport from finite one-, two-, and three-dimensional sources in a finite-thickness aquifer.

Journal of Contaminant Hydrology. 53(1-2): 41-61. DOI: 10.1016/S0169-7722(01)00136-X.

Saffi, M. and Cheddadi, A. 2007. Explicit algebraic influence coefficients: a one-dimensional transient aquifer model. Hydrological Sciences Journal. 52(4): 763-776. DOI: 10.1623/hysj.52.4.763.

Sahimi, M. 2003. Heterogeneous materials. I. Springer-Verlag, New York.

Sanskrityayn, A., Sul, H. and Kumar, N. 2017. Analytical solutions for solute transport in groundwater and riverine flow using Green's Function Method and pertinent coordinate transformation method. Journal of Hydrology. 547: 517-533. DOI: 10.1016/j.jhydrol.2017.02.014.

Torquato, S., Kim, I.C., Cule, D. 1999. Effective conductivity, dielectric constant, and diffusion coefficients of digitized media via first-passage time equations. Journal of Applied Physics. 85: 1560. DOI: 10.1063/1.369287.

Wu, J.C. and Zeng, X.K. 2013. Review of the uncertainty analysis of groundwater numerical simulation. Chinese Science Bulletin. 58(25): 3044-3052. DOI: 10.1007/s11434-013-5950-8.

Yeh, W W-G. 2015. Review: Optimization methods for groundwater modeling and management. Hydrogeology Journal. 23: 1051–1065. DOI: 10.1007/s10040-015-1260-3.

Zhang, D. 2001. stochastic methods for flow in porous media: Coping with Uncertainties. Academic Press. ISBN: 9780127796215.